

Experimental and statistical investigation of torque coefficient in optimized surface piercing propeller

Masoud Zarezadeh^a, Nowrouz Mohammad Nouri^{*} and Reza Madoliat^b

School of Mechanical Engineering, Iran University of Science and Technology, Narmak, Heydarkhani St., Tehran, 16846-13114, Iran

(Received December 12 2023, Revised January 19, 2024, Accepted January 20, 2024)

Abstract. The interaction of the blade of surface-piercing propellers (SPPs) with the water/air surface is a physical phenomenon that is difficult to model mathematically, so that such propellers are usually designed using empirical approaches. In this paper, a newly developed mechanism for measuring the torque of SPPs in an open water circuit is presented. The mechanism includes a single-component load cell and a deformable torque sensor to detect the forces exerted on the propeller. Deformations in the sensor elements lead to changes in the strain gauge resistance, which are converted into voltage using a Wheatstone bridge. The amplified signal is then recorded by a 16-channel data recording system. The mechanism is calibrated using a 6-DoF calibration system and a Box-Behnken design, achieving 99% accuracy through multivariate regression and ANOVA. Finally, the results of performance tests on a 4-blade propeller were presented in the form of changes in the torque coefficient as a function of feed rate. The results show that the new mechanism is 8% more accurate than conventional empirical methods.

Keywords: experimental test; manufacturing; statistical study; surface-piercing propellers

1. Introduction

Surface-piercing propellers (SPP) are mainly used in flat boats, where they reduce the drag acting on the propeller

by about 30%, reduce erosion caused by cavitation, and improve the efficiency of speedboats and fast ships (Carlton 2018). SPPs enable a larger propeller radius due to their distance from the stern of the boat and their high power generation capacity. However, due to their limited application, there is little published information on SPP geometries and comprehensive data (Lorio 2010). Designers have sought to gain a more comprehensive understanding of position variables (yaw angle, angle of attack, the ratio of submergence) and their effects on the performance of SPPs (Ferrando and Scamardella 1996). The costly and difficult process of testing full-scale propellers emphasizes the need to test model propellers in different configurations to investigate the effects of operating parameters on SPPs. Due to the challenges and costs associated with testing full-scale propellers,

*Corresponding author, Professor, E-mail: mnouri@iust.ac.ir

^aPh.D. Student

^bProfessor

researchers have focused on developing experimental facilities for model testing of SPPs in laboratories (Kruppa 1975, Liu and Zhu 1988).

(Hecker and Crown 1970, Ferrando and Scamardella 1996, Kikuchi *et al.* 1999, Peterson 2005, Pustoshny and Rusetsky 2006, Ding 2007) published the results of their experimental studies. In their study, these researchers investigated the performance of SPP at different advance rates and characterized the areas of full and partial aeration. In another part, they investigated the model test of SPPs to determine the factors affecting these propellers. The results showed that the significant effects of the Froude, Weber, and cavitation numbers on the generalizability of the results obtained from the model SPP test could be transferred to the full-scale SPP. (Ferrando *et al.* 2007) analyzed the effects of shaft angle, submersion level, and blade pitch in five-blade propellers. They modified definitions and coefficients were used to develop a regression model for thrust, torque coefficients, and critical advance rate. Experimental studies focus on the design and fabrication of model test mechanisms to adjust propeller position and measure forces and torques. There are various approaches, such as using force-torque sensors attached to the propeller shaft to accurately measure the force components (Kikuchi *et al.* 1999), installing a multi-component transducer attached to the hub and connected to a blade, (Olofsson 1996), and attaching a strain gauge to the blades (Nozawa and Takayama 2002). Depending on their capabilities, the measurement methods can measure propeller thrust, reaction torque and lateral forces.

According to (Bahaj *et al.* 2007), designing and commissioning a dynamometer involves predicting forces and torques, selecting appropriate materials and strain gauges and ensuring sensitivity without unwanted thrust or creep. This enables accurate measurement of thrust and torque. (Funeno *et al.* 2013) designed a torque measurement system for the SPP spindle. He focused on embedding thrust and torque measurement sensors in the propeller shaft connection and integrating a spindle torque measurement sensor in the propeller hub. The sensors were connected to a data logger system via a hollow axis, and a belt motor drove the propeller shaft. (Shafaghat 2016) presented the calculation and fabrication of various elements comprising a closed cavitation tunnel with free surface to measure the thrust force and torque acting on the SPP of a two-component dynamometer. A review of the relevant literature shows that various geometrical and positional parameters influence the performance and hydrodynamic behavior of the SPP. However, the published works (Bose *et al.*) did not present a comprehensive method to predict the performance of the SPP and explain the effects of the different parameters on this property. (Chen *et al.* 2018) investigated the hydrodynamic efficiency of a submarine propeller (E1619) under unrestricted flow conditions. They found that scaling up the model propeller to full scale had significant effects on the torque coefficient and pressure distribution, emphasizing the importance of sizing in studying the hydrodynamic performance of SPP. (Seyyedi *et al.* 2019) conducted a study to investigate the effects of degree of submergence and pitch angle on the hydrodynamic coefficients of SPPs. The results showed that increasing the immersion level and shaft angle resulted in higher propulsive force, rotational force and torque. (Ha *et al.* 2023) investigated the performance of a surface-piercing propeller (SPP) in open water. They found that the propeller exhibited thrust reduction and aeration phenomenon, resulting in additional thrust loss, especially at lower advance rates. The lack of standardized procedures and experimental tests for surface-piercing propellers (SPPs) makes it difficult to predict their performance and analyze the effects of the parameters at the design stage. There is a need for specific experimental test systems to investigate the effects of geometric and positional factors in the design of SPPs (Brookshire 2022, Eskandari and Ghassemi 2022).

As can be seen from previous research, the measurement of hydrodynamic parameters is important and the development of a mechanism to measure these parameters is essential. The design

of the SPP torque measurement requires careful consideration of blade motion, fluctuating loads, and environmental conditions. In this study, a mechanism for measuring torque in a water tunnel was developed and calibrated to investigate the hydrodynamic characteristics of four-bladed SPPs. A cost-effective average torque measurement system was developed to circumvent the need for expensive rotating instruments in the empirical analysis of SPPs. The propeller was tested in the IUST water tunnel and the effects of submergence ratio and axial inclination on the torque coefficient were analyzed. The aim of the study was to investigate the hydrodynamic properties of SPPs and to present the results graphically.

2. Test setup and propeller model

The IUST open-circuit water tunnel was designed to enable hydrodynamic investigations and to carry out the necessary tests in a test section. The tunnel consists of an open segment with dimensions of 200×150 mm, which allows adjustable water velocities between 2 and 6 m/s. It includes a test area, a water pump, a flow meter, an open channel for water transportation and a storage tank for water supply and venting. A flow control segment was integrated into the system to create a uniform flow pattern and control turbulence in both the longitudinal and transverse directions of the tunnel (Lumley and McMahon 1967, Mehta and Bradshaw 1979). This segment consists of a honeycomb layer and two wire mesh layers designed to improve turbulence control in the flow. A converter then transforms the cross-section of the round metal tube into a 2 m long, rectangular Plexiglas channel. The flow passing through this section improves the alignment of the flow within the test area. The current flowing through this segment improves the alignment of the flow within the test area. Here, the water moves to another rectangular section that narrows and has a flexible top plate designed to mimic the configuration of the hull of high-speed ships. The water then moves to an open test section with a free surface where the propeller is located. After passing through the test section, the water continues to flow through a U-shaped channel that leads into the open channel below the pipeline. Finally, it flows back to the expansion tank and the pumps, completing the water cycle.

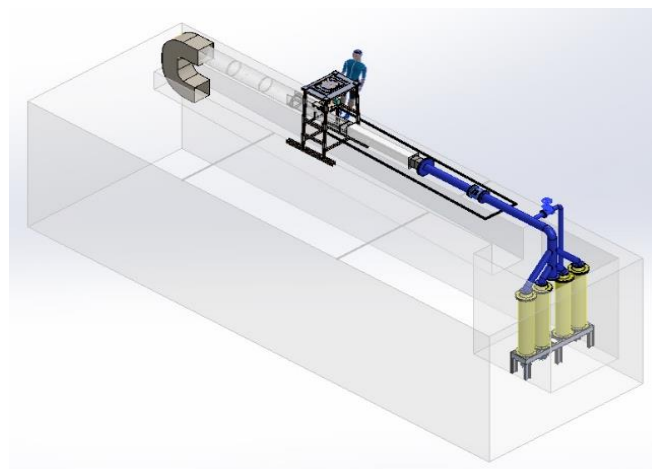


Fig. 1 Closed circuit water tunnel of IUST

The tunnel utilizes four submerged pumps connected via pipes and a five-way manifold. It offers yaw angles and angles of attack up to 8° , immersion ratios up to 100%, and a circular-section channel leading to an open-water channel for water circulation. The schematic of tunnel is demonstrated in Fig. 1. This tunnel can generate a flow velocity of 2 to 10 m/s in the test section with a length of 1.5 m.

3. Design criteria

To minimize the noise in the torque signal, the design focused on increasing the applied forces while reducing the

errors associated with the noise. Shortening the torque arm increased the applied force and improved the signal-to-noise ratio. In this research, a lever mechanism was used to transfer the torque to the arm, which contained nested holes for measuring the torque at different lengths. A torque sensor with resilient components was used to counteract the reaction forces of the motor. A pulley system to which an S-type load cell was connected to measure the force. The resulting force multiplied by the distance gave the torque value. Strain gauges on flexible elements recorded the deformation, and the amplified signal was analyzed with a data acquisition system to measure the applied forces.

Optimal section sizes and positions for the strain gauges were determined iteratively to achieve a maximum output signal of 2 mV/V , with a tolerance of $\pm 16\%$ and a maximum deformation of $10^3 \text{ } \mu\epsilon$. Eq. (2) relates the strain at a specific section to the output signal from the Wheatstone bridge.

$$U/U_e = 1/4k(\epsilon_1 - \epsilon_2 + \epsilon_3 - \epsilon_4) \quad (1)$$

The bending stress at the deformation sensor position is calculated as a function of the deformation, represented by " ϵ ", and the gauge parameter, denoted as " k ".

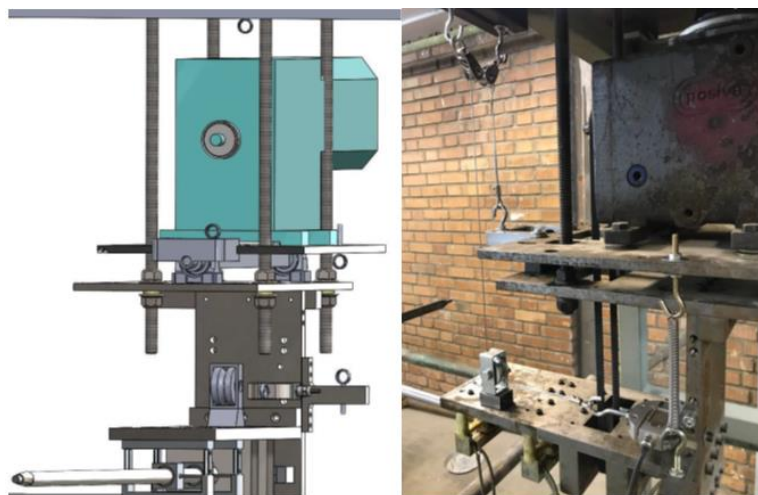


Fig. 2 Mechanism of torque measurement

$$\sigma = M \frac{I}{c} \quad (2)$$

where $\frac{I}{c}$ represents the bending resistance and M denotes the torque at the location of the strain gauge. The measurement strain can then be calculated from the relationship between the flexural stress and the elasticity modulus (E), as per Eq. (3)

$$\varepsilon = \sigma/E \quad (3)$$

For optimal output voltage, a balanced Wheatstone bridge configuration with strain gauges was used, ensuring equal strain and allowing calculation of the output signal using Eq. (4).

$$\Delta U/U = k\varepsilon \quad (4)$$

By substituting strain values and material properties into Eq. (3), design stress can be computed for the maximum load at the strain gauge position, which is then used in Eq. (2) to determine appropriate dimensions for the measurement section (Bartz and Blatz 2022).

3.1 Pulley-string system

In this study, a pulley system was used to transmit only the axial tensile force to the S-type load cell, which is ideal for measuring axial force. In contrast to rigid mechanisms, this system also avoids non-axial forces caused by vibrations. A woven tension wire with a diameter of 1.5 mm and a load capacity of 300 kg was used together with several steel rollers and a pulley. The tension wire is connected to the arm and load cell with a clamp, camlock coupling and standard size 6 screw anchors (see Fig. 2).

3.2 Establishing the preload mechanism

Since the cable hoist is only designed for tensile forces and does not react to compressive forces and the motor plane can rotate freely, the fluctuations in the motor torque were damped by connecting a spring with a certain stiffness to the motor plane via a tensioned arm. This allowed a predetermined preload to be applied to the system through the tension cable bracket (see Fig. 3).

3.3 Railed mechanism

To enable tests with different arm lengths, a rail system with an iron box profile was implemented. A trench was created in the middle of the profile in which the rollers could move freely. However, the problem arose that the rollers were neither suspended nor fixed. To solve this problem, the trench was extended and the pulley suspension was moved away from the opening for the wire passage. This adjustment ensured that the wire formed a normal angle with the arm when the pulley was set at 45° (see Fig. 4).

3.4 Sliding mechanism of pulleys

To ensure that only an axial force was applied to the load cell, an additional deflection pulley was fitted underneath the system, through which the tension cable was passed before it reached the load cell. This created ideal conditions for force measurement (see Fig. 5).



Fig. 3 Primary load mechanism



Fig. 4 Railed mechanism for changing the arm length



Fig. 5 Sliding mechanism of pulleys



Fig. 6 Propeller model test mechanism calibration system

4. Calibration of the propeller test mechanism

In order to analyze the forces and torques obtained from the output voltage of the sensors, the system as a whole must be calibrated. The purpose of calibration is to estimate the sensitivity and response behavior of the sensors. Calibration is performed using the Hydrotech Center's six-degree-of-freedom calibration system, which allows simultaneous loading at 6DoFs with no system rotation and minimal mechanical components. Fig. 6 shows a general view of the calibration system of the balance, and the orientation of the measuring system is shown in Fig. 7.

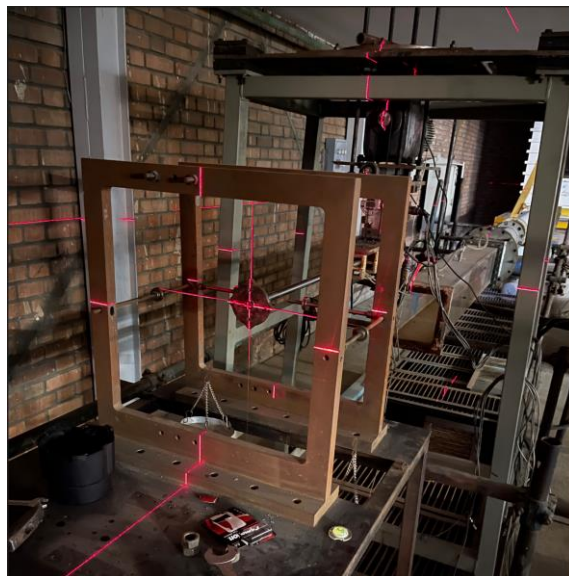


Fig. 7 Alignment of measurement system

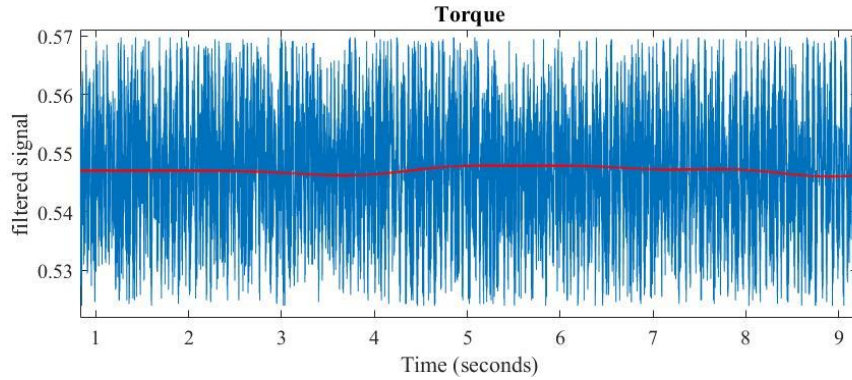


Fig. 8 A typical torque signal at submerge rate 0.6 and advance ratio 0.8

Table 1 The error rate of predictive modeling for signal pathways

Source	Response
Contribution	Torque
Model	99.94%
Linear	99.95%
Error	0.015%
Lack-of-Fit	0.00%

A calibration test matrix was designed according to the principles of the Response Surface Methodology (RSM), which follows the Box-Behnken design. This approach enabled the statistical analysis of linear and non-linear effects as well as the accuracy and repeatability of data from different channels. After applying mixed loads according to the schedule, the data acquisition system recorded output signals at a sampling rate of 10 Hz, which were filtered, time-averaged and statistically analyzed for calibration purposes. A typical torque signal is shown in Fig. 8.

In this paper, a quadratic polynomial regression equation (Eq. (5)) was used to develop the empirical model that represents the numerical relationship between the input factors and the output variables through a mathematical formula.

$$R_i = \sum_{j=1}^4 A_{ij}S_j + \sum_{j=1}^4 C_{ij}S_j^2 + \sum_{j=1}^4 \sum_{k=j}^4 B_{ijk}S_jS_k \quad (5)$$

Regression coefficients included 1st-degree impacts of each load (A_{ij}), 2nd-degree (C_{ij}), and interaction impact between variables (B_{ijk}) and the effective coefficients of each response were used to analyze the effects of the different loadings on the response variables. ANOVA was performed to assess the significance of each independent parameter. All expressions were analyzed with a p-factor at a significance level of 95 percent. The final model was evaluated using the correlation coefficient (R^2), the normal probability plot and the residual error analysis. Finally, appropriate coefficients were extracted to identify significantly effective parameters for each channel (Eq. (6)).

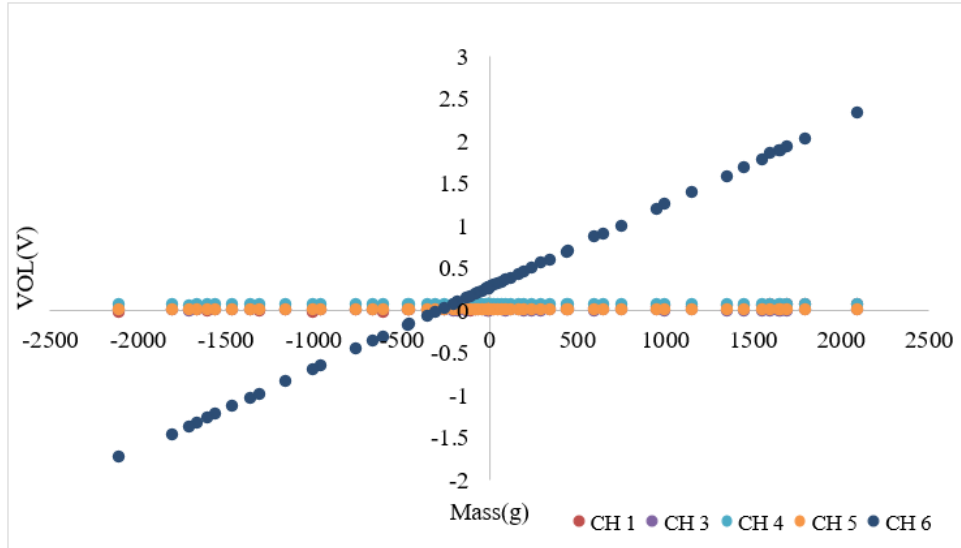


Fig. 9 Torque sensor sensitivity

$$C = \begin{bmatrix} -0.928 & 0 & 0.0851 & 0 \\ 0 & -0.9629 & 0 & 0 \\ 0.0118 & 0.0053 & -1.412 & 0 \\ 0 & 0 & 0 & 1.5 \\ 0 & 0 & 0 & 0 \\ 0 & 0.01647 & 0 & 0 \\ 0 & 0 & -0.0343 & 0 \\ 0 & 0 & 0 & 0 \\ 0 & 0 & 0 & 0 \\ -0.0128 & 0 & 0 & 0 \\ 0 & 0 & 0 & 0 \\ 0 & -0.0204 & 0 & 0 \\ 0 & 0 & 0 & 0 \\ 0 & 0 & 0 & 0 \end{bmatrix} \tag{6}$$

Table 1 shows that the prediction accuracy of the modeling for the torque signal pathway is above 99.90%. The total error, consisting of residual and fitting error, is less than 1% for all signal pathways, indicating high precision and consistency of the sensors and accurate load prediction with the regression model.

Fig. 9 shows the behavior of the individual channels in response to changes in torque in order to investigate the linear behavior of the sensor in the corresponding load range. The results of these experiments show that the sensor exhibits accurate linear behavior and effectively discriminates the design load.

5. Positional parameters and propeller model data

The basic parameters in relation to a propeller, namely the dimensionless torque coefficients as the power factor to be evaluated in relation to the propulsion coefficient.

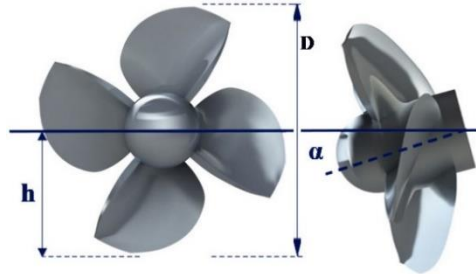


Fig. 10 The immersion depth and shaft attack angle in relation to the free surface

Table 2 Specification of SPP propeller

Parameters	Amount
Diameter (m)	0.13
Number of blades	4
Chord length (0.7R)	0.421
Hub-diameter ratio	0.3
Expanded area ratio	0.67
Pitch Ratio	1.24

$$J = \frac{V_a}{nD} \quad (7)$$

$$K_Q = \frac{Q}{\rho n^2 D^5} \quad (8)$$

The parameters that determine the position of the propeller examined in this study are the angle of attack of the shaft and the immersion depth, which is shown in Fig. 10.

$$I_T = \frac{h_T}{D} \quad (9)$$

Table 2 presents the details of the propeller and Fig. 11 shows picture of SPP model.



Fig. 11 The optimized SPP model



Fig. 12 The flow pattern in $J=1$, $Fr=4$

6. Experiment tests

After completing the calibration of the system's sensors and determining the load-voltage relationships, the customized test setup was implemented in the water channel facility and empirical tests were conducted to investigate the SPP test procedure at three different immersion ratios ($I = h/D = 0.32, 0.4, 0.6$ and 0.75) and three shaft angles ($\alpha = 3, 6$ and 8°). Based on the given criteria and ranges for model similarity, the rotation speed of the propeller was set to 2158-3419 rpm, considering a propeller diameter of 13 cm. The selected range for the advance rate was $0.25 \leq J \leq 1.4$. Based on the theories of Ding and Dyson (Dyson 2000, Ding 2007) with the defined range of Froude ($Fr_n > 3.65$), Weber > 200 , Reynolds $> 5 \times 10^5$ numbers, it is found that dynamic similarity exists. Finally, the test matrix is shown in Table 3.

The flow pattern around the propeller at $Fr=4$ and $J=1$ is shown in Fig. 12. At this advance coefficient, the efficiency of the propeller is at its highest and, as can be seen, the air cavities are more complete. The pattern of the ventilation cavity and wake can be observed, as the cavity is shorter and the wake diameter reduces downstream far the propeller.

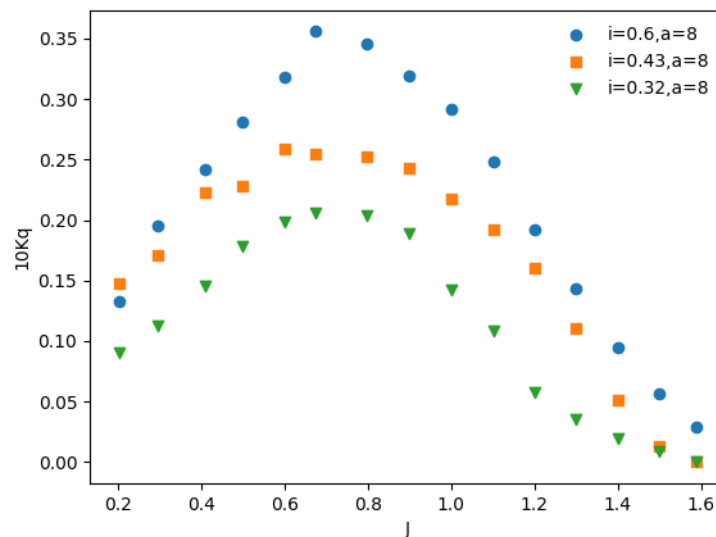
7. Operating SPP test mechanism

After completion of the experimental tests, an analysis was carried out to investigate the hydrodynamic behavior of the model propeller. The torque acting on the propeller was determined by using calibration equations. The results were presented in the form of dimensionless torque coefficients. To illustrate this, Fig. 8 shows the signal output of the torque sensors (shown in blue) over a 10-second interval with a frequency of 10 kHz.

After time averaging and filtering, the resulting signal (shown in red) was used to derive the time-averaged coefficients. Fig. 13 shows the torque coefficients of the model propeller at different immersion ratios. These graphs illustrate the significant influence of immersion depth on the performance of surface-piercing propellers. The data shows that the torque coefficients decrease

Table 3 Test Matrix

D(m)	J	Q(m ³ /h)	U(m/s)	N(rpm)
0.13	0.25	200	1.85	3419
	0.3			2849
	0.35			2442
	0.4			2137
	0.45	350	3.24	3324
	0.5			2991
	0.55			2720
	0.6			2493
	0.65	500	4.63	2301
	0.7			2137
	0.75			2849
	0.8			2671
	0.85	707	6.55	2514
	0.9			2374
	0.95			2249
	1			2137
	1.05	707	6.55	2035
	1.1			2747
1.15	2627			
1.2	2518			
1.25	707	6.55	2417	
1.3			2324	
1.35			2158	
1.4			2158	

Fig. 13 The influence of vary submerge ratio on torque factor in shaft inclination angle 8°

with decreasing immersion ratios. This reduction is attributed to the decrease in the impressive zone of the propeller. The coefficient curve agrees with the experimental results published by other researchers (Olofsson 1996, Dyson 2000). To ensure the reproducibility of the test system, the test matrix of the propeller was repeated three times. The largest error in reproducibility, about 10 percent, occurred in the transition region. This result was attributed to the instability of the ventilation in this area. In addition, the influence of forced ventilation on the hydrodynamic properties of this propeller was investigated using the SPP current loop mechanism, as described by Amini and colleagues (Amini *et al.* 2021). Their results showed that the performance improvement of the propeller decreases with increasing immersion ratio. Furthermore, the range associated with improved performance shifted to higher propulsive coefficients.

8. Results

The ratio of immersion depth to propeller diameter is one of the most important factors influencing the development and efficiency of surface propellers. The axial pitch of the shaft, the immersion ratio, can be influenced by factors such as the boat trim and the performance of the propeller at different advance coefficients and can therefore be precisely controlled. In order to investigate the effect of this parameter separately, immersion tests were carried out at different shaft inclination angles. Looking at Fig. 13, which shows the effect of variations in the immersion ratio at a fixed shaft angle of 8° on the shaft at constant coordinates, the torque coefficient decreases as the immersion level decreases. This decrease is due to the reduced effective surface area of the propeller. The relationship of K_q is shown as a box plot in Fig. 14.

Median of the torque coefficient at 8° shaft angle and immersion rate of 0.6 was about 0.24 with an IQR range of 0.12 – 0.32. With decreasing the immersion ratio to 0.43, the median decreased to about 0.17 with an IQR range of 0.13 – 0.25. When the immersion rate was reduced to 0.32, the median torque coefficient reached 0.08, and IQR range touched 0.04 – 0.12. As is evident from the box plot, the highest IQR range corresponded to the 0.6 immersion rate rather than the other two

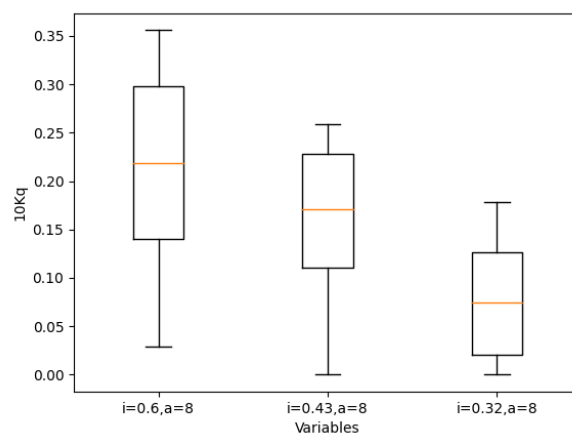
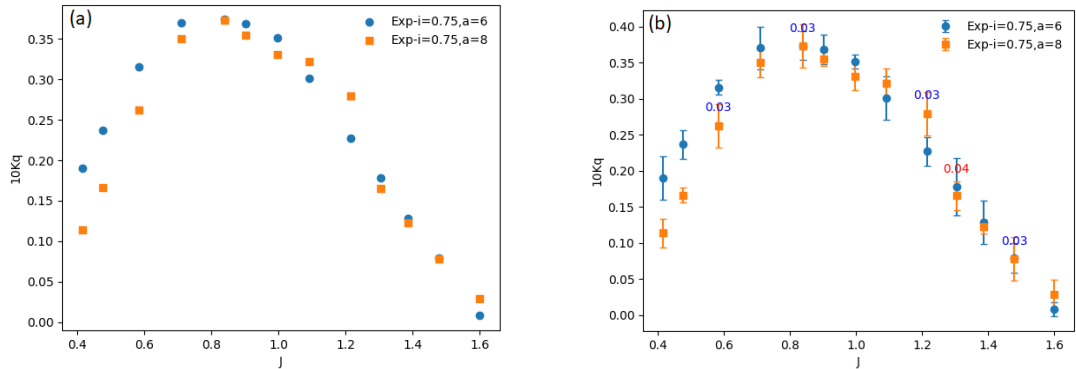


Fig. 14 The distribution of k_q in difference immersion ratio dataset, showing the median, quartiles, and any outliers as boxplot



(a) impact of varying angle of shaft inclination on torque factor

(b) error bar of difference between $a=6$ and $a=8$

Fig. 15 Effect of angle of shaft inclination and related error bar in submerge ratio 0.43

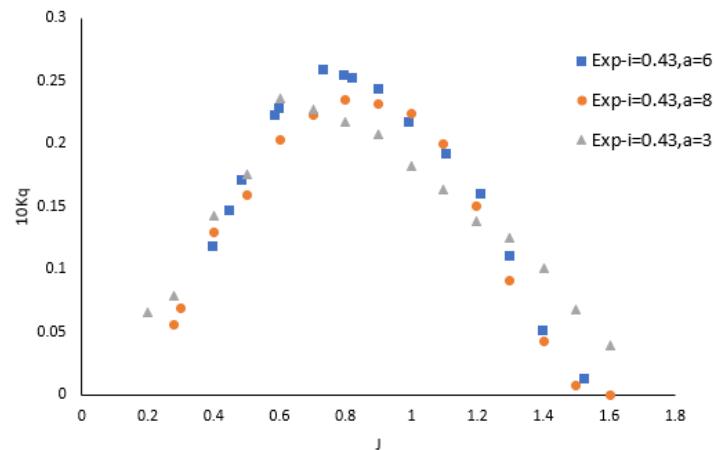


Fig. 16 influence of varying angle of shaft inclination on torque factor in submerge ratio 0.43

values. In the meantime, the 0.6 immersion rate exhibited a higher median torque than the other two values. As is evident, higher torque coefficients were observed at a higher immersion ratio.

Fig. 15 reveals the influence of the SPP angle of shaft on the torque factor considering the shaft coordinate as fixed at a fixed submerge ratio of 0.75. According to Fig. 16, the torque coefficient increases with increasing the shaft angle. This coefficient increases only slightly when the shaft angle increases from 6 to 8°. The relationship of Kq in various shaft angles is depicted as a boxplot in Fig. 17.

The median of the torque coefficient at 6° shaft angle was about 0.22 with an IQR range of 0.15 – 0.25. With increasing the shaft angle to 8°, the median decreased to about 0.15 with an IQR range of 0.07 – 0.20. When the shaft angle was reduced to 3°, the median torque coefficient reached 0.17,

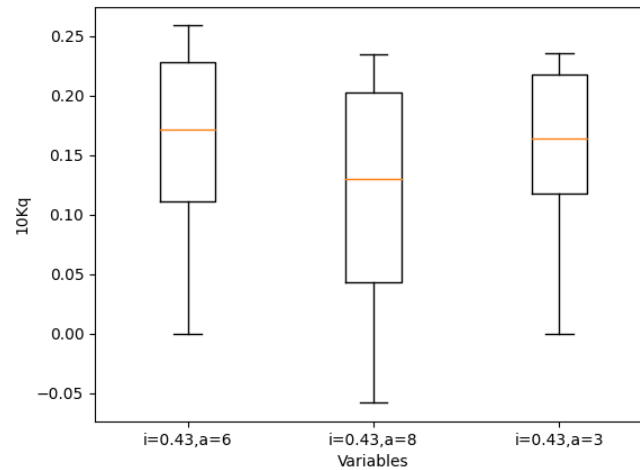


Fig. 17 the distribution of Kq in difference shaft inclination angle dataset, showing the median, quartiles, and any outliers as boxplot in $i=0.43$

and IGR range touched 0.12 – 0.21. As is evident from the box plot, the torque coefficients exhibited some normal distribution and the highest IQR range corresponded to the 8° shaft angle rather than the other two values. In the meantime, the 6° shaft angle exhibited a higher median torque than the other two values. As is evident, higher torque coefficients were observed at higher shaft angles.

To investigate the effect of factors together, a correlation analysis is performed, The Correlation matrix provides a general view to the correlation of the torque coefficients at various angles of shaft and submerge ratios. On the pairwise comparison matrix of these variables, each element indicates the correlation coefficient of a pair of data points. Based on this matrix, the torque coefficients at the immersion ratio of 0.43 and shaft angles of 6 and 8° are strongly and positively correlated to one another, indicating a significant association between the corresponding variables. The torque coefficients at the immersion ratio of 0.43 and shaft angles of 6 and 3° are moderately yet positively correlated to one another, indicating some mild association between the corresponding variables. Similarly, the torque coefficients at the immersion ratio of 0.43 and shaft angles of 8 and 3° are moderately and positively correlated to one another, indicating some mild association between the corresponding variables. The obtained values of the torque factor at an immersion rate of 0.43 and a shaft angle of 8° was found to be weakly yet positively correlated to the one at an submerge ratio of 0.6 and a shaft angle of 6°, which implies a subtle association. The obtained values of the torque factor at an immersion ratio of 0.43 and a shaft angle of 6° was found to be weakly yet positively correlated to the one at an immersion ratio of 0.6 and a shaft angle of 6°, which implies a subtle association. The obtained values of the torque coefficient at a fixed shaft angle of 6° but immersion rate of 0.32 and 0.43 exhibited some weak yet positive correlations, which implies a subtle association (see Fig. 18).

Based on results, the correlation drops as one changes either of the angle of shaft and the submerge level, and stronger correlations are expected when the angle of shaft and the submerge level fall in the same range.

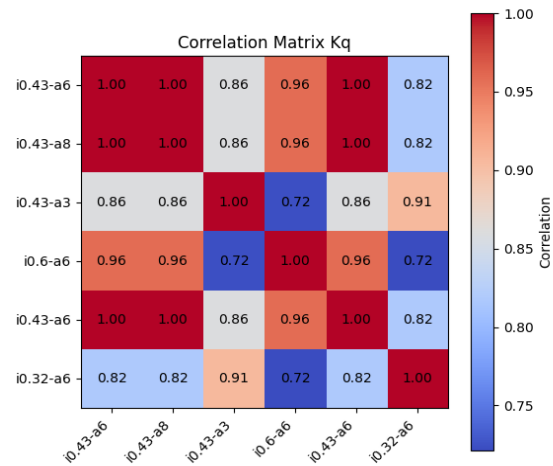


Fig. 18 the correlation matrix of Kq in difference angle of shaft inclination and difference submerge level

Table 4 The t-test results between torque coefficients

	Kq-i0.6, a=8		Kq-i0.43, a=6		Kq-i0.43, a=8		Kq-i0.32, a=6		Kq-i0.32, a=8	
	t-statistic	p-value	t-statistic	p-value	t-statistic	p-value	t-statistic	p-value	t-statistic	p-value
Kq-i0.6, a=6	0.281	0.781	1.368	0.181	2.460	0.020	2.494	0.018	1.644	0.110
Kq-i0.6, a=8			1.019	0.316	2.083	0.046	2.124	0.042	1.266	0.215
Kq-i0.43, a=6					1.263	0.216	1.330	0.194	0.210	0.835
Kq-i0.43, a=8							0.113	0.911	-1.185	0.245
Kq-i0.32, a=6									-1.257	0.219
Kq-i0.32, a=8										

Table 4 reports the results of the t-test on the torque coefficients. As the table suggests, the obtained p-values indicate that average torque coefficients are not significantly different when one of the two parameters remain the same (e.g., shaft angles of 6 and 8° at the fixed submerge ratio of 0.6, or submerge ratio of 0.43 and 0.6 at constant shaft angle of 6°).

This means that the variables mentioned are likely to lead to similar average values. If the ranges of both parameters differ simultaneously (e.g., when comparing a certain immersion ratio at a certain shaft angle with another immersion ratio associated with a different shaft angle), the average values start to differ significantly. For example, the torque coefficients corresponding to $[a = 6, Kq-i = 0.6]$ and $[a = 8, Kq-i = 0.43]$ differed significantly with a p-value of 0.020, indicating that these two torque coefficients would have significantly different average values. Further results can be found

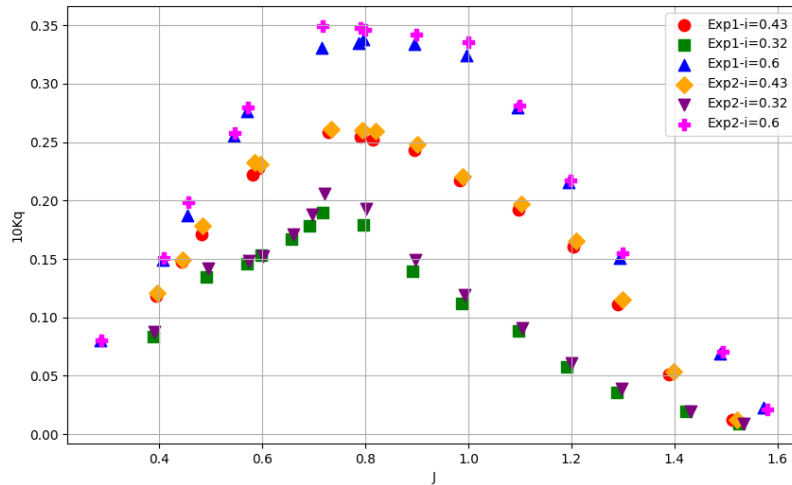


Fig. 19 the comparison of Kq for two tests conducted at different immersion ratios

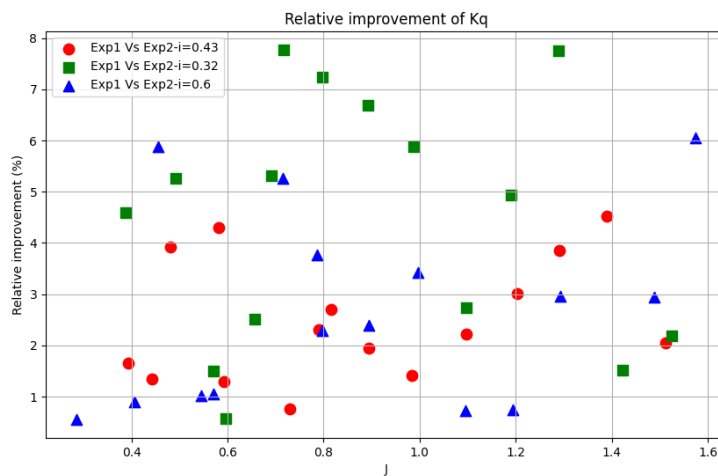


Fig. 20 the relative improvement of Kq based on J

in Table 4. Finally, to investigate the effect of introducing a new mechanism for measuring the torque coefficient compared to the existing results at the IUST Hydrotech Center, two test results are compared in Fig. 19.

In Fig. 19, Exp1 refers to existing experimental data at the Hydrotech Center (Kamran *et al.* 2022), while Exp2 represents a new test performed in the IUST water tunnel. The improvement in the measurement of Kq is shown as a relative improvement based on different J at different immersion rates (Fig. 20). The results show that the maximum improvement of Kq is about 8%.

Previously, the torque was measured using the reaction torque generated by the motor resting on a moving plate that rests on a bearing aligned with the center of the motor and transmits the torque to the connected S-type load cell.

9. Conclusions

In order to conduct experimental studies on SPPs to investigate the influences of position and operating variables on the torque coefficient, model tests were carried out in the IUST water tunnel and a mechanism for measuring the reaction torque acting on the propeller was designed and manufactured. The proposed system was calibrated via the BBD using a 6-DoF calibration mechanism. A statistical analysis and multivariate regression were then performed to determine the calibration factors with an error rate of less than 1%. The results showed good resolution and linearity of the sensors. The effects of two position parameters, namely the immersion ratio and the shaft angle, on the torque coefficient were subjected to further statistical analysis. The results showed that the torque coefficient increases with increasing immersion ratio, while increasing the shaft angle resulted in only a slight increase in the torque coefficient. Comparison of the obtained torque coefficients with those obtained by experiments at IUST's Hydrotech Center confirmed that the proposed torque measurement mechanism improved the measurement accuracy by 8%.

Acknowledgments

We are grateful to the Hydrotech Group, which operates in the field of scientific technologies.

Disclosure statement

The authors report there are no competing interests to declare.

References

- Amini, A., Nouri, N.M., Abedi, A. and Kamran, M. (2021), "Performance improvement of surface piercing propeller at low advance coefficients by aeration", *Ocean Eng.*, **238**, 109551. <https://doi.org/10.1016/j.oceaneng.2021.109551>.
- Bahaj, A., Molland, A., Chaplin, J. and Batten, W. (2007), "Power and thrust measurements of marine current turbines under various hydrodynamic flow conditions in a cavitation tunnel and a towing tank", *Renew. Energ.*, **32**(3), 407-426. <https://doi.org/10.1016/j.renene.2006.01.012>.
- Bartz, J.R. and Blatz, J.A. (2022), "Considerations for measuring residual stresses in driven piles with vibrating wire strain gauges", *Can. Geotech. J.*, **59**(3), 441-446. <https://doi.org/10.1139/cgj-2020-0614>.
- Bose, N., Dugué, C., Esposito, P.G., Holtrop, J., Jessup, S., Lee, J.T., Mewis, F., Poustoshny, A., Salvatore, F. and Shirose, Y. "The Propulsion Committee".
- Brookshire, K. (2022), An Analysis on Hydrodynamic Loads for Surface-Piercing Propellers Using Computational Fluid Dynamics, Virginia Tech.
- Carlton, J. (2018), Marine propellers and propulsion, Butterworth-Heinemann.

- Chen, X., Huang, Y., Wei, P., Zhang, Z. and Jin, F. (2018), "Numerical analysis of scale effect on propeller E1619", International Conference on Offshore Mechanics and Arctic Engineering, <https://doi.org/10.1115/OMAE2018-78213>.
- Ding, E. (2007), "A series of surface piercing propellers and its application", *Proceedings of the 9th International Conference on Fast Sea Transportation*, Shanghai, China.
- Dyson, P.K. (2000), "Modelling, testing and design, of a surface piercing propeller drive".
- Eskandari, M. and Ghassemi, H. (2022), "A simple practical method to show the forces of the surface propeller during one cycle", *Am. J. Mech. Eng.*, **10**(1), 34-40.
- Ferrando, M., Crotti, S. and Viviani, M. (2007). "Performance of a family of surface piercing propellers", *Proceedings of the 2nd International Conference on Marine Research and Transportation (ICMRT)*, Ischia.
- Ferrando, M. and Scamardella, A. (1996), "Surface piercing propellers: Testing methodologies, results analysis and comments on open water characteristics".
- Funeno, I., Pouw, C. and Bosman, R. (2013). "Measurements and computations for blade spindle torque of controllable pitch propellers in open water", *Proceedings of the 3rd International Symposium on Marine Propulsors smp*.
- Ha, J., Park, J., Park, G., Kim, J., Kim, J., Seo, J. and Rhee, S.H. (2023), "Experimental study on the propulsion performance of a partially submerged propeller", *Int. J. Naval Architect. Ocean Eng.*, **15**, 100516. <https://doi.org/10.1016/j.ijnaoe.2023.100516>.
- Hecker, R. and Crown, D. (1970), "Performance characteristics of partially-submerged propeller 4281 with varying number of blades at low advance coefficients", NSRDC T and E Report.
- Kamran, M., Nouri, N.M., Goudarzi, H. and Golrokhifar, S. (2022), "Experimental evaluation of the effect of positioning and operating parameters on the performance of a surface-piercing propeller", *Scientific Reports*, **12**(1), 18566. <https://doi.org/10.1038/s41598-022-21959-x>.
- Kikuchi, H., Sasaki, N., MURAKAMI, K., KIHARA, H., YABUSHITA, K. and SUZUKI, K. (1999), "Experimental study on surface piercing propeller with axis horizontally raked", *J. Kansai Soc. Naval Archit. Jpn.*, 1-8.
- Kruppa, C. (1975), "Propulsion devices for high-speed craft (Testing techniques)", *Proceedings of the 14th international towing tank conference (Report of cavitation committee)*, Ottawa, ON, Canada.
- Liu, S. and Zhu, H. (1988), "An experimental study on the performance characteristics of partially submerged propeller", *Proceedings of the International High Performance Vehicle Conference*.
- Lorio, J.M. (2010), Open water testing of a surface piercing propeller with varying submergence, yaw angle and inclination angle, Florida Atlantic University
- Lumley, J.L. and McMahan, J. (1967), "Reducing water tunnel turbulence by means of a honeycomb".
- Mehta, R.D. and Bradshaw, P. (1979), "Design rules for small low speed wind tunnels", *Aeronaut. J.*, **83**(827), 443-453.
- Nozawa, K. and Takayama, N. (2002), "Experimental study on propulsive performance of surface piercing propeller", *J. Kansai Soc. Naval Archit. Jpn.*, 63-70.
- Olofsson, N. (1996), "Force and ow characteristics of a partially submerged propeller doctoral thesis", Goteborg: Chalmers University of Technology {Department of Naval Architecture and Ocean Engineering.
- Peterson, D.T. (2005), Surface piercing propeller performance, Citeseer
- Pustoshny, A. and Rusetsky, A. (2006), "Naval and commercial fast ship development experience and further prospects", *Aust. J. Mech. Eng.*, **3**(2), 79-90. <https://doi.org/10.1080/14484846.2006.11464497>.
- Seyyedi, S.M., Shafaghat, R. and Siavoshian, M. (2019), "Experimental study of immersion ratio and shaft inclination angle in the performance of a surface-piercing propeller", *Mech. Sci.*, **10**(1), 153-167. <https://doi.org/10.5194/ms-10-153-2019>.
- Shafaghat, R. (2016), "Design algorithm of a free surface water tunnel to test the Surface-Piercing Propellers (SPP); Case study water tunnel of Babol Noshirvani university of technology", *Int. J. Maritime Tech.*, **6**, 19-30. <https://doi.org/10.18869/acadpub.ijmt.6.19>.

Nomenclature

K_T	Thrust coefficient
K_Q	Torque coefficient
J	Advance coefficient
W_n	Weber number
ρ_v	Vapor pressure of water
σ_0	Cavity number
Fr_n	Froud number
l_T	Immersion depth
D	Propeller diameter
Re_n	Reynolds number
ψ	Yaw angle
α	attack angle
AE/AO	Surface area ratio (Expanded area/Disk Area)
η	Propeller efficiency
Fr_n	Propeller Froude number
V	Advance velocity
Z	Number of blades
n	Rotation rate
ρ	Mass density of water
g	Gravitational constant
h_T	Propeller immersion depth
ν	Kinematic viscosity
E	Elasticity module
T	Thrust
Q	Torque
P_0	Static pressure on Free surface water